ACS APPLIED MATERIALS & INTERFACES

Research Article

www.acsami.org

Fine-Tuning the Surface of Forward Osmosis Membranes via Grafting Graphene Oxide: Performance Patterns and Biofouling Propensity

Hanaa M. Hegab,[†,‡] Ahmed ElMekawy,[§,∥] Thomas G. Barclay,[⊥] Andrew Michelmore,[⊥] Linda Zou,[†,#] Christopher P. Saint,[†] and Milena Ginic-Markovic*[,⊥]

[†]Centre for Water Management and Reuse, University of South Australia, Adelaide SA 5095, Australia

[‡]Institute of Advanced Technology and New Materials, City of Scientific Research and Technological Applications, Borg Elarab, Alexandria, Egypt

[§]Genetic Engineering and Biotechnology Research Institute, University of Sadat City (USC), Sadat City, Egypt

[∥]School of Chemical Engineering, University of Adelaide, Adelaide SA 5095, Australia

[⊥]Mawson Institute, University of South Australia, Adelaide, SA 5095, Australia

[#]Department of Chemical and Environmental Engineering, Masdar Institute of Science and Technology, Abu Dhabi, United Arab Emirates

ABSTRACT: Graphene oxide (GO) nanosheets were attached to the polyamide selective layer of thin film composite (TFC) forward osmosis (FO) membranes through a poly L-Lysine (PLL) intermediary using either layer-by-layer or hybrid (H) grafting strategies. Fourier transform infrared spectroscopy, zeta potential, and thermogravimetric analysis confirmed the successful attachment of GO/PLL, the surface modification enhancing both the hydrophilicity and smoothness of the membrane's surface demonstrated by water contact angle, atomic force microscopy, and transmission electron microscopy. The biofouling resistance of the FO membranes determined using an adenosine triphosphate bioluminescence test showed a 99% reduction in surviving bacteria for GO/PLL-H modified membranes compared to pristine membrane. This antibiofouling property of the GO/PLL-H modified membrane was reflected in reduced flux decline compared to all other samples when filtering brackish water under biofouling conditions. Further, the high density and tightly bound GO nanosheets using the hybrid modification reduced the reverse solute flux compared to the pristine, which reflects improved membrane selectivity. These results illustrate that the GO/PLL-H modification is a valuable addition to improve the performance of FO TFC membranes.

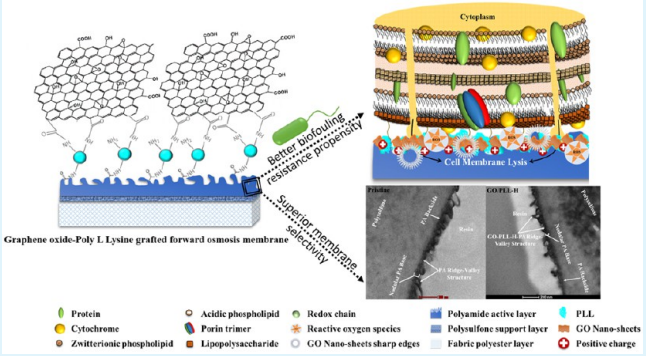

KEYWORDS: *graphene oxide, forward osmosis, antifouling, grafting, thin film composite membrane*

1. INTRODUCTION

Osmotically driven membranes have the potential to address the issues of global water scarcity by incorporation into water purification processes.[1] This has promoted considerable research interest into the application of forward osmosis (FO) in industrial and environmental wastewater purification. Despite the recent advances in FO technology, it still suffers from several major limitations, which highlights the need for improving membrane design including ways to reduce membrane fouling and methods to minimize the loss of draw solute.[2−4]

Biofouling is an inevitable aspect to membrane filtration. Biofouling initiates through the accumulation and growth of microorganisms on the surface of the membrane, starting the development of a biofilm.[5] Stages for the formation of such biofilm include (1) bacterial cell attachment, (2) cell to cell adhesion, (3) proliferation, (4) maturation, and (5) dispersion of planktonic bacteria.[6−8] Once the biofilm is stabilized on the membrane surface (via weak hydrogen bonding and van der Waal's, hydrophobic, or electrostatic interactions) it works as a bioreactor, at the wrong time and place, leading to undesired water flux decline and overall higher energy consumption.[9,10] Although it was reported that fouling of FO membrane is reversible[1] compared to ultrafiltration (UF), nanofiltration (NF), and reverse osmosis (RO) membranes, biofouling is considered as an obstacle that limits the use of FO membrane filtration, in particular, for wastewater feed applications without pretreatment.[2−4] Several approaches have been suggested to control and minimize the FO membrane fouling phenomenon. Examples include, developing innovative setups for the FO module, optimization of FO operation conditions, partial prepurification of feed solution, cleaning with chemical agents,

Received: June 2, 2015
Accepted: July 27, 2015
Published: July 27, 2015

DOI: 10.1021/acsami.5b04818
ACS Appl. Mater. Interfaces 2015, 7, 18004−18016

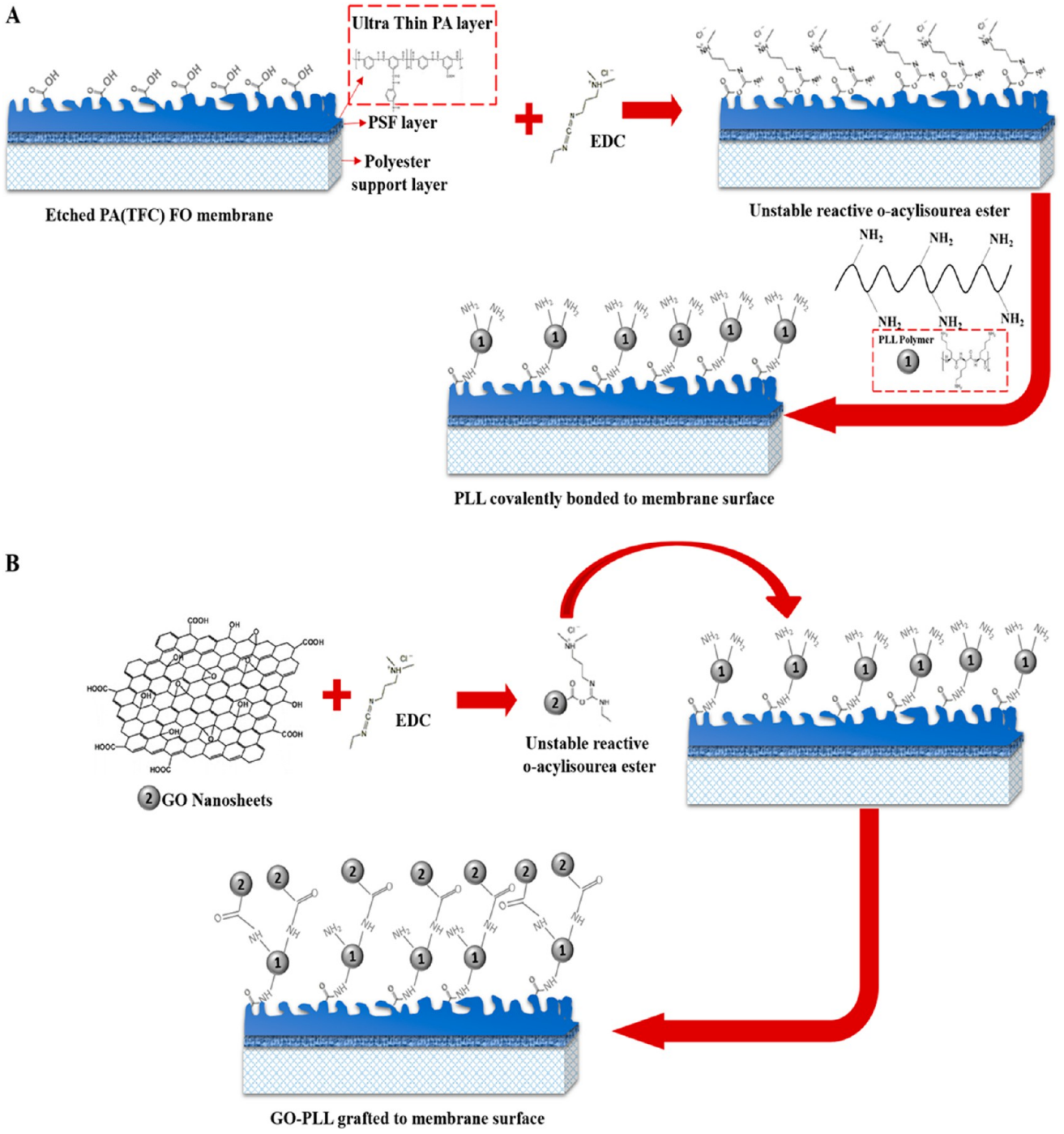

Figure 1. Schematic chemical reaction of GO/PLL-LbL membrane surface modification technique: (A) PLL covalently binding to the native carboxyl moieties of polyamide FO (TFC) membranes and (B) GO assembled on the surface of PLL modified FO membrane.

using spacers, and membrane surface modifications.[11−13] While all these methods have value, the easiest and most efficient antifouling strategy that can be easily applied to current FO membrane manufacture and filtration plant technologies is surface modification.

Another challenge in the design of the FO membranes that can be addressed using surface modification is the development of a highly selective thin film composite (TFC) active layer. Generally, TFC-FO membranes have moderate selectivity compared to state of the art seawater TFC-RO membranes.[14,15] This low selectivity in FO membrane processes is due to a high rate of reverse solute flux (J_s), which also accelerates the onset of membrane fouling.[16] Once the reverse solute passes through the PA selective layer, it leads to the undesirable diffusion of solute, an increase in the internal concentration polarization (ICP) and blockage of the membrane porous layer.[17] Moreover, the ICP has a more prominent negative influence on the water flux of FO process, compared to the effect of external concentration polarization.[18,19] Thus, a tight active layer is required for low reverse salt diffusion and fouling.[20]

Recently, the unique attributes of amphilphilic GO nanosheets promoted a new generation of high water flux membranes. GO nanosheets deposited on the membrane substrate have the ability to form laminate space, resulting in

DOI: 10.1021/acsami.5b04818
ACS Appl. Mater. Interfaces 2015, 7, 18004−18016

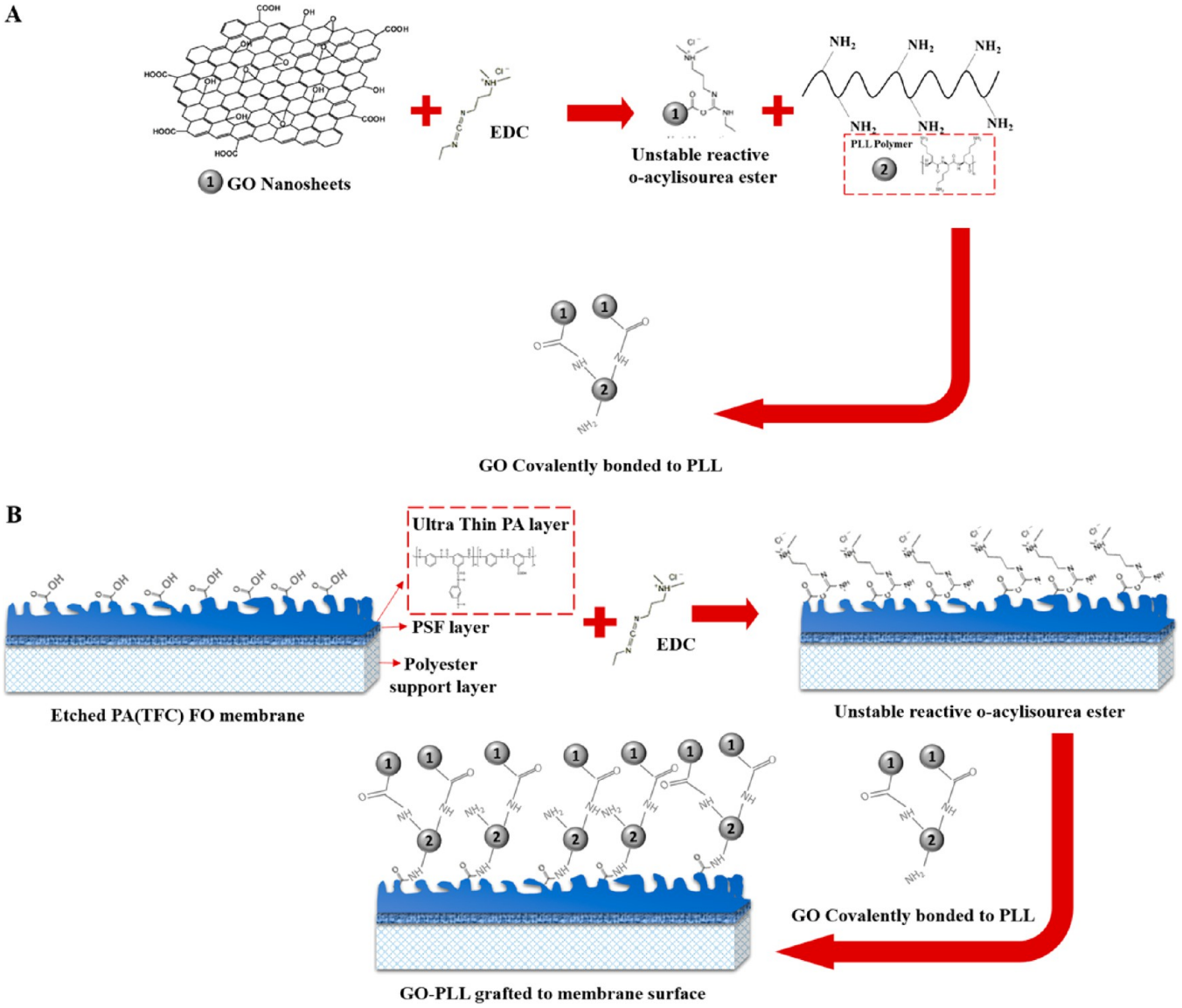

Figure 2. Schematic chemical reaction of GO/PLL-H membrane surface modification method: (A) GO covalently bonded to PLL and (B) the hybrid GO-PLL covalently binding to the native carboxyl moieties of polyamide FO (TFC) membranes.

channels that filter water with frictionless diffusion.[21,22] To take advantage of these attributes of GO nanosheets, it is also imperative to maintain the suitability of any GO-based membrane for use in water filtration applications. Therefore, the utilization of the common and simple filtration method to fabricate GO-based membranes[23,24] carries the environmental risk of dispersion of hydrophilic GO nanosheets into the hydrosphere. This risk is mitigated by fabricating GO nanosheets that are strongly bound to each other and to the support substrate, previously addressed by two main strategies.[25] One strategy is based on stacking the negatively charged GO nanosheets, through electrostatic interaction onto a positively charged layer.[26,27] The other approach is the formation of covalent bonds between the GO layers by applying cross-linkers such as trimesoyl chloride (TMC).[28] In addition to the benefits to filtration performance, GO nanosheets also have bactericidal and fungicidal properties[29,30] that could be leveraged for reducing biofouling.

Although several research projects have studied FO membrane biofouling,[31−33] limited attention has been given to both rectifying the problem of FO membrane reverse solute flux drawback and designing effective methods to inhibit the bacterial growth on the membrane surface using an easily applied coating. Herein, we report two different strategies for grafting the surface of FO membrane; layer by layer (LbL) or hybrid (H) layers of GO nanosheets/PLL, to form a stable modified surface of GO/PLL-LbL or GO/PLL-H membranes in order to compare their performance and biofouling resistance in FO mode. We then analyzed the pristine and coated membranes to confirm the successful grafting of GO/PLL, studying the structure, topography, thermal stability, surface coating density, antibacterial, hydrophilicity, and surface charge properties of the membranes.

2. MATERIALS AND METHODS

2.1. Synthesis of GO Nanosheets and Grafting of FO Membranes. GO nanosheets was prepared by chemical exfoliation (modified Hummer's technique) of Gt (graphite powder SP-1 < 20 μm; Bay Carbon, Bay City, MI). The reaction mechanism was reported in our previous study.[12]

DOI: 10.1021/acsami.5b04818
ACS Appl. Mater. Interfaces 2015, 7, 18004−18016

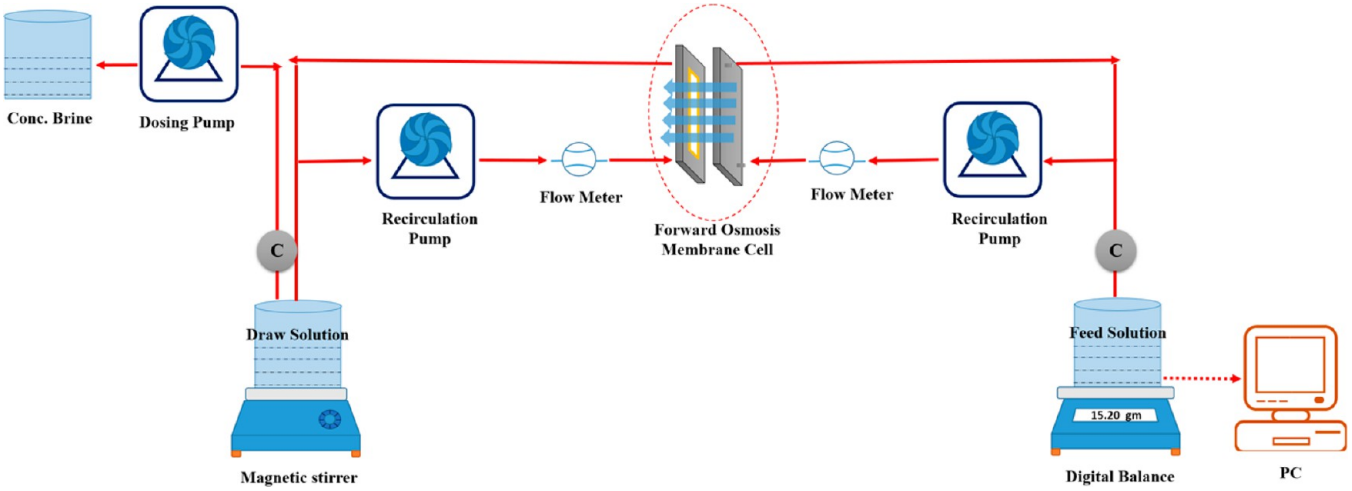

Figure 3. Schematic diagram of experimental FO setup.

GO nanosheets are used to modify the surface of FO TFC membranes through layer-by-layer (LbL) or hybrid (H) techniques. To assemble GO/PLL-LbL onto an FO (TFC) membrane, we sandwiched the membrane between a backing plate and a frame made of poly(methyl methacrylate) to expose only the active layer. The membrane surface was then etched with 200 ppm sodium hypochlorite for 2 min followed by washing with Milli-Q water from ultrapure water purification system (Millipore, Synergy). A solution of 60 mM 1-ethyl-3-[3-(dimethylamino) propyl] carbodiimide hydrochloride 98% (EDC) (Sigma-Aldrich TM) was prepared with pH adjusted to 5.5 using HCl/NaOH and placed onto the membrane surface for 15 min, altering the carboxyl groups of the PA active layer into amine-reactive esters, as indicated in (Figure 1). The EDC solution was then replaced with an aqueous solution of PLL (500 μg/mL) (Sigma-Aldrich TM) prepared in water for 30 min and then removed. Graphene oxide (80 μg/mL) was dispersed in EDC (4 mM) solution at pH 5.5 by sonication for 10 min and then placed onto the PLL-grafted TFC membrane. The GO/PLL-LbL grafted membranes were rinsed with Milli-Q water several times to remove any unbound GO from the membrane surface and stored in Milli-Q water at 4 °C until used. A similar procedure was applied to graft hybrid GO/PLL on the membrane surface (Figure 2). In brief, a covalently bound hybrid between GO nanosheets and PLL was formed first from an aqueous dispersion, and then the GO/PLL hybrid was grafted to the activated FO membrane surface for 30 min.

2.2. Characterization of FO Membranes and GO Nanosheets. Zeta potential measurements were conducted to determine the surface charge of pristine and grafted membranes using an Anton Paar SurPASS Electrokinetic Analyzer (Anton Paar, Austria) with adjustable gap cell height. The streaming current was determined and the Helmholtz–Smoluchowski approximation was utilized to calculate the zeta potential. For all experiments, 10 mM of potassium chloride (KCl) solution was used as the background. Measurements were performed over a pH range of 9–3. Starting with pH value of approximately 9, adjusted by 0.1 M sodium hydroxide (NaOH), the pH gradually dropped to 3, using dosing pump that automatically injects calculated amounts of 0.1 M hydrochloric acid (HCl). The zeta potential instrument was set to collect four data points at every 0.5 pH increment and report the average.

The chemical composition of the surface of pristine and grafted membranes were examined by attenuated total reflectance Fourier transform infrared spectroscopy (ATR-FTIR), using a Nicolet Nexus 8700 FTIR Spectrophotometer (Thermo Electron Corporation) fitted with a Smart Orbit ATR accessory, including a diamond crystal internal reflection element. Data generated were manipulated using OMNIC software.

Thermogravimetric analysis (TGA Discovery) was employed to analyze the material composition of grafted membranes. The samples were placed in the platinum pans and heated from 30 to 700 °C at 10 °C/min and under a flow of N_2 (25 mL/min). The temperature calibration was performed using the Curie temperatures of nickel and alumel standard reference materials (TA Instruments). To find the GO nanosheets graft density, we used the same area of the membranes for TGA analysis. The weight change of the PLL modified membrane was subtracted from the weight change of GO/PLL-H and GO/PLL-LbL in the region of 250–600 °C, to give the mass per area of grafted GO.

AFM (NT-MDT NTEGRA SPM) in noncontact mode was used to compare the roughness of pristine and grafted membranes. A tip of silicon nitride coated with gold on the reflective side (NT-MDT, NSG03) was utilized. The scanner, calibrated by 1.5 μm standard grids having height of 22 nm with resonance frequencies from 65 to 100 kHz, has a maximum range 100 μm. The oscillation amplitude was utilized in 10 nm with a scan rate of 0.5 Hz. Then, 3 μL of GO suspension in water (5 μg/mL) was dropped on a 1 cm^2 silicon wafer for measuring the dimension of GO nanosheets.

The morphology of the grafted and pristine membranes were studied using micrographs of their respective cross sections captured by transmission electron microscopy (FEI Tecnai G2 Spirit TEM). The sample preparation protocol consisting of immersion of the membrane in white resin for at least 24 h, before embedding it into gelatin capsule, packed with resin to eliminate oxygen exposure, and cured overnight at 60 °C. Cross sections were prepared using a Leica Ultra cut ultra microtomer with a diamond knife and inserted into carbon/Formvar (polyvinyl formal) coated copper grids.[34]

The Data-Physics OCA15 Contact Angle Analyzer (Data Physics Instruments GmbH, Filderstadt, Germany) was used to measure the surface wettability of pristine and grafted membranes. The captive bubble method was utilized for measuring the contact-angle. The drop images were captured and angles calculated by OCA software. At least five replicates were used for each measurement, and the average values were reported.

2.3. Evaluation of FO Membrane Performance. Membranes were assembled in FO mode to compare the performance of pristine and modified membranes, as illustrated in Figure 3. Flat sheet TFC FO membrane (HTI, OsMem TFC Membrane) with an effective surface area of 48 cm^2 was used. Mesh spacer (low foulant spacer, Sterlitech, WA) was positioned on both sides of the holder to support the membrane with the same surface area. Milli-Q water or 5 g/L NaCl solution, was used as feed solution for each experiment. Peristaltic pumps (Cole-Parmer, Australia) and flow meters (Cole-Parmer, Australia) were employed to push the feed and draw solutions with a flow rate of 500 mL/min on both sides of the membrane.

The draw solution concentration was kept constant for all experiments (2 M NaCl, prepared from analytical reagent grade NaCl (Ajax Finechem Pty. Ltd., Australia) through a dosing pump,

DOI: 10.1021/acsami.5b04818
ACS Appl. Mater. Interfaces 2015, 7, 18004–18016

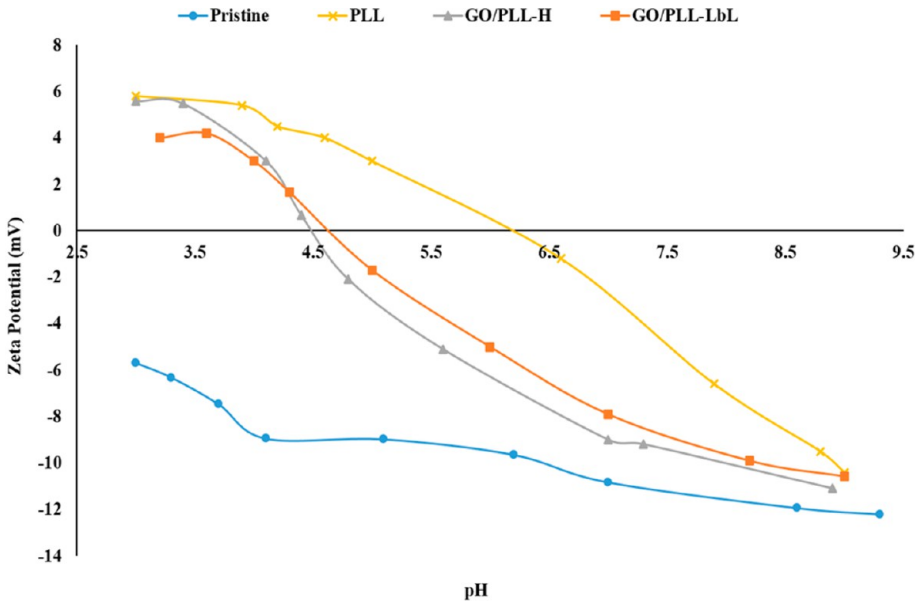

Figure 4. Zeta potential of pristine and modified FO membranes.

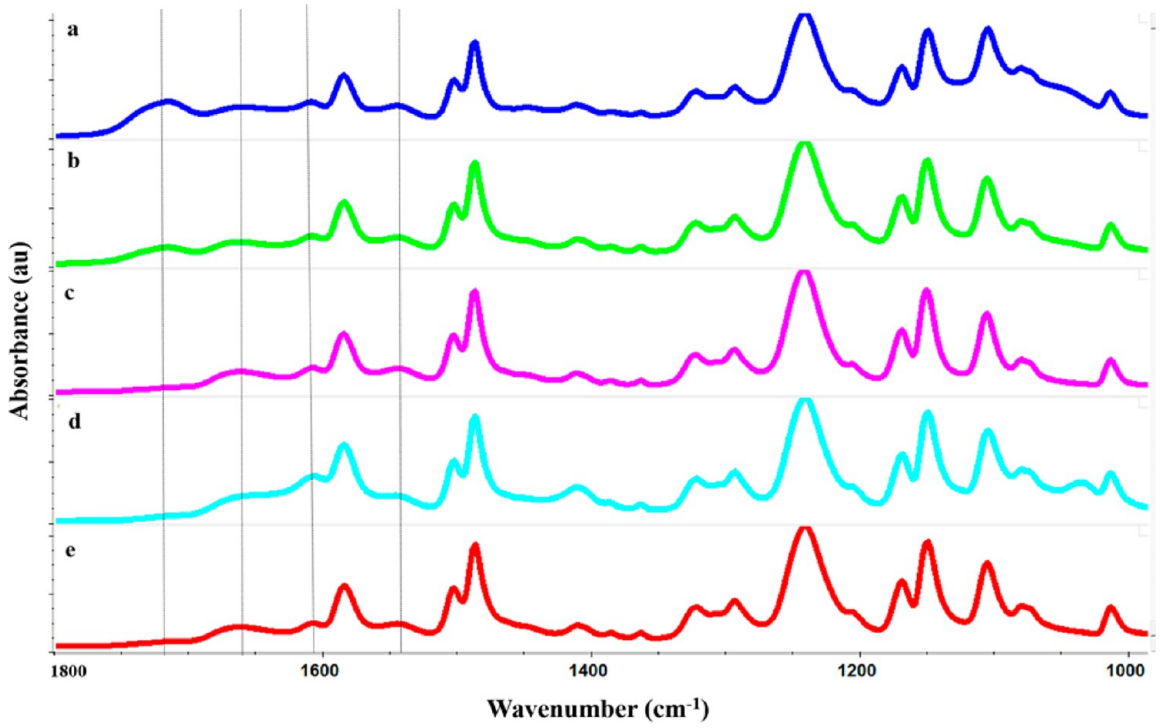

Figure 5. ATR-FTIR spectra of (a) pristine, (b) etched, (c) PLL, (d) GO/PLL-H, and (e) GO/PLL-LbL membranes in the range of 1000−1800 cm^{-1}.

connected with a conductivity sensor to avoid changing the osmotic pressure. A digital balance (MS 1600 l, Mettler-Toledo, Switzerland) connected to a computer recorded the weight of water permeate as a function of time. The water flux (J_w, in units of L m^{-2} h^{-1}) was measured by the volume change of permeate, as given by eq 1.[33]

$$J_w = \frac{\Delta \text{volume of permeate}}{\text{membrane surface area} \times \Delta \text{time}} \quad (1)$$

2.4. Biofouling of FO Membranes and Cleaning Procedure. Prior to each experiment, the FO setup was washed using 0.25% sodium hypochlorite solution for 30 min, then with Milli-Q water for 30 min. Then membranes were installed and rinsed in Milli-Q water at a cross-flow rate of 9.9 cm/s for 30 min before running for 23 h using the NaCl (2M) draw solution described above and a fouling feed solution. The feed solution was natural brackish surface water from a local Australian lake spiked with nutrient to enhance the bacterial growth rate and accelerate the biofouling on the membrane surface. This spiked feed solution was composed of 2 g/L of sodium acetate (Merck, Australia), 0.6 g/L sodium nitrate (Ajax Chemical, Ltd., Australia) and 0.2 g/L of sodium dihydrogen phosphate (May and Baker, Ltd., England), producing a C/N/P mass ratio of 100:20:10.[33] The permeate water flux was automatically recorded using a digital balance connected to a computer. To clean fouled membranes, both feed and draw solutions were replaced by Milli-Q water at flow rate of 1000 mL/min for 1h. To assess flux recovery after cleaning, we then

DOI: 10.1021/acsami.5b04818
ACS Appl. Mater. Interfaces 2015, 7, 18004−18016

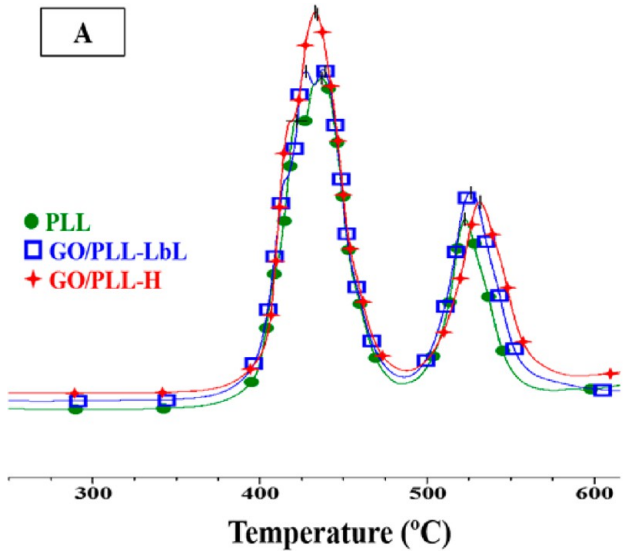

B

Sample	Wt Change (mg)	GO Grafting Density (mg/cm²)
PLL	1.75	0
GO/PLL-H	1.87	0.2
GO/PLL-LbL	1.79	0.08

Figure 6. TGA of PLL, GO/PLL-H, and GO/PLL-LbL grafted FO membranes. (A) The growing peak at ~440 °C corresponds to increasing GO nanosheets on the FO membrane surface and (B) the GO grafting density values on the membrane surface.

tested all membranes again for 1 h filtration in FO mode using Milli-Q water as a feed solution, and NaCl (2 M) as a draw solution.

2.5. Biofouling Analysis. To quantitatively determine the biocidal activity of collected biofouled membrane samples, we conducted accurate and fast Adenosine Tri Phosphate (ATP) biochemical test to measure the concentration of live biological cells. The main concept of ATP analysis is measuring the quantity of light, created via enzymatic reaction, by using the luciferin−luciferase assay in alumina meter calibrated with solutions of free ATP (Celsis) in sterilized water (Celsis Advance).[35,36] The samples for ATP test were prepared by scraping fouled membrane surface from a specific surface area on all samples. The samples were then diluted in 50 mL of sterilized water before the ATP analysis. To quantify the free ATP of fouled membranes, we placed samples in the polystyrene tube of ATP kit and positioned in the auto sampler chain. The ATP dispenser automatically injects certain ratios of (Celsis, LuminEX) to lyse the bacterial membrane of the cells, followed by luciferin−luciferase (Celsis, Lumin ATE) into the mounted samples. The detection limit of this setup is 1 ng/L of the measured sample.

3. RESULTS AND DISCUSSION

3.1. Membrane Surface Charge. Zeta potential curves, revealed in Figure 4, provide information on the surface charge distribution for pristine and surface modified membranes as a function of pH. The zeta potential of pristine FO membrane was negative over the entire tested pH range.[37] Coating the membrane with PLL cationic polymer significantly shifted the zeta potential and iso-electric point compared to the unmodified membrane, making it positively charged at acidic pH. This was due to the presence of secondary and primary amino groups on the membrane surface that were able to take on a positive charge.[38] For membranes modified with both PLL and GO nanosheets the zeta potential is positive at the most acidic pH due to the PLL, but the presence of the negatively charged oxygen functional groups on GO nanosheets surface incorporated by either technique (LbL or H) resulted in zeta potential levels in the entire pH range that are intermediate between that of pristine and PLL treated membranes. Lastly, the slightly more negative zeta potential for GO/PLL-H coatings compared to GO/PLL-LbL coatings indicates a greater GO grafting density on the hybrid membrane surface, further validated by the TGA analysis (Figure 6B)

3.2. Surface Functional Groups. The ATR-FTIR spectra of the pristine, etched and surface modified FO membranes are shown in Figure 5. The ATR-FTIR spectrum in Figure 5a shows the typical peaks of an aromatic polyamide layer. The peaks at 1663 and 1541 cm^{-1} represent the amide I (C═O stretch) and amide II (N−H bending) respectively, while the peak at 1609 cm^{-1} represents the C═C stretching of an aromatic amide.[12] Characteristic peaks in the spectrum of etched membrane (Figure 5b) were not discernably different to the pristine membrane except for the reduction in the intensity of the C═O stretching of benzoic acids at 1710 cm^{1},[39] which is attributed to the breakage of hydrogen bonds between C═O and N−H groups.[40] The successful grafting of PLL, GO/PLL-H, and GO/PLL-LbL and stable covalent bond formation with the membrane surface is evidenced by the amide-I bands (1663 cm^{-1}) shift to a higher peak intensity. It is postulated that this is due to the formation of covalent amide bonds between native carboxyl groups of FO membrane and amino groups of PLL (Figure 5c) or between the carboxyl groups of GO nanosheets, amino groups of PLL, and activated FO membrane surface (Figure 5d,e). The fact that the spectra over the range of 1145−1350 cm^{-1} in the polysulfone layer remains unaltered, confirms that the NaOCl etching did not degrade the polysulfone layer.[39]

3.3. Thermal Analysis. The presence of GO and PLL on the membrane surface was also confirmed using thermogravimetric analysis (TGA). The thermograms of surface modified membranes in the temperature range of 250−600 °C are presented in Figure 6A. There are two significant peaks in the first derivative of the mass loss curves. The largest one appears in the temperature range of 350−475 °C and is associated with the degradation of the selective amide layer and components of the support layer of the underlying membrane as well as the applied coating. The presence of two small peaks and the shoulder within the first significant peak confirms the successful surface modification of the polyamide layer with GO/PLL-LbL and GO/PLL-H, respectively, and is in agreement with reported literature.[41] The second peak occurs at 520 °C as a result of the degradation of the supporting polysulfone layer.[42]

The grafting density of GO nanosheets on the FO membrane surface was calculated based on the TGA data and is presented

DOI: 10.1021/acsami.5b04818
ACS Appl. Mater. Interfaces 2015, 7, 18004−18016

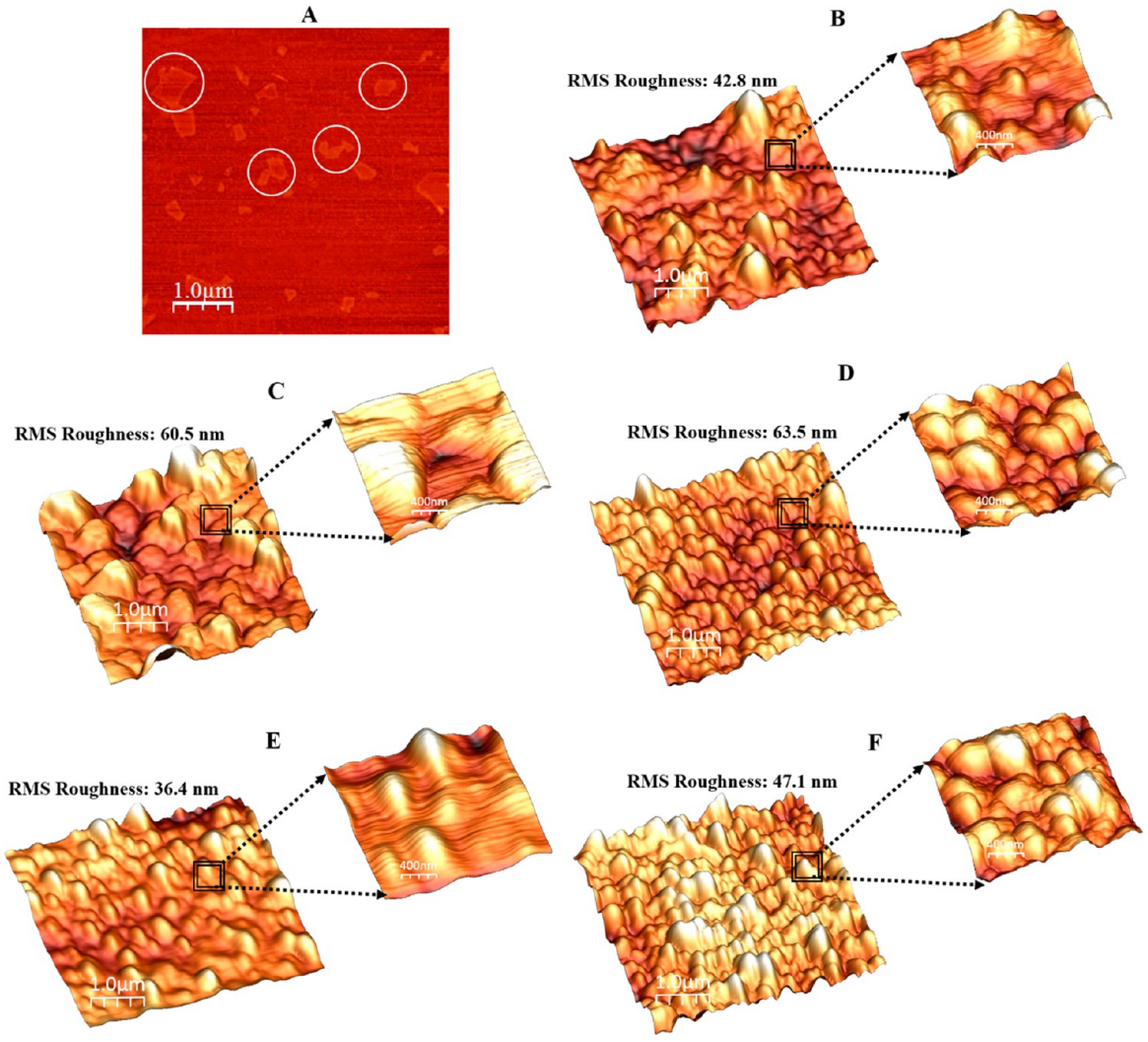

Figure 7. AFM 2D image of (A) GO nanosheets and 3D images of (B) pristine, (C) etched, (D) PLL, (E) GO/PLL-H, and (F) GO/PLL-LbL membranes.

in the inset table in Figure 6B. The graft density of GO nanosheets on the FO membrane surface prepared via the hybrid method is higher than that prepared by LbL technique. It is hypothesized that the reaction between dissolved polycationic PLL and dispersed GO nanosheets in the hybrid technique presents ideal access between the amine and EDC activated carboxyl functional groups, maximizing the amount of GO attached. In contrast, in the LbL technique the GO nanosheets can only covalently bind the exposed amino groups of the PLL surface layer. Grafting density results are consistent with zeta potential results, in which GO/PLL-H showed a more negatively charged surface throughout the pH range.

3.4. AFM Analysis. AFM was used to confirm the successful fabrication of the GO and to measure their dimensions. The thickness of single GO Nanosheet was in the range between 1.5 and 2.5 nm with lateral dimension in the range between 200 and 1000 nm (Figure 7A). AFM was also used to compare the roughness profile of the pristine, etched, and grafted membrane surfaces (Figure 7B–E). The surface roughness of pristine FO membrane was relatively uniform with root-mean-square (RMS) of 43 nm. Etching of the membranes leads to a rougher surface (61 nm, RMS), the morphological difference helping to verify the chemical change. The PLL coating does not significantly change the roughness of the etched surface (63 nm, RMS) suggesting that the PLL is conformally attached to the membrane surface, creating a monolayer which follows the substrate "hills" and "valley" rough configuration. In contrast, the grafted GO/PLL-H and GO/PLL-LbL exhibited smoother surface topography of 36 and 47 nm (RMS), respectively. The smoother surface morphology of the grafted GO/PLL coatings is conceivably due to the GO nanosheets occupying the valleys of the grafted PLL. This illustrates that the GO/PLL modification does not significantly change the surface roughness of the unmodified membranes. This is important because rough surface morphology increases the membrane surface area, increasing binding sites for bacterial adhesion,[43,44] and decreases the effectiveness of hydrodynamic cleaning of the fouled biofilm layer on the membrane surface.[44]

3.5. Morphology of Modified FO Membranes. TEM images of the cross sections of the pristine PA, NaOCl etched, grafted PLL, GO/PLL-H and GO/PLL-LbL composite membranes are shown in Figure 8. The morphology of the PA skin layer is a function of the chemical cross-linking reaction rate and the formation of covalent and hydrogen bonds.[45] Etching of the membrane with sodium hypochlorite and the

DOI: 10.1021/acsami.5b04818
ACS Appl. Mater. Interfaces 2015, 7, 18004–18016

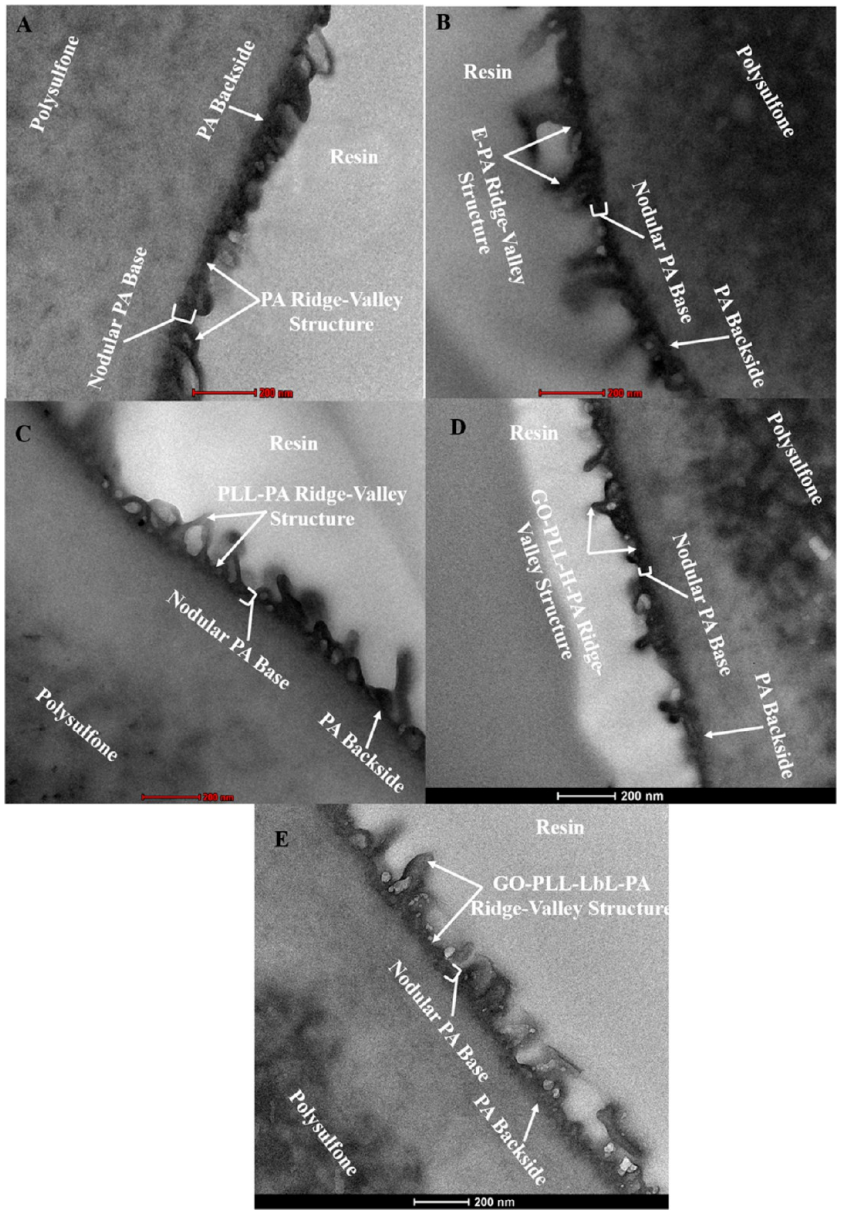

Figure 8. TEM images of the cross sections of (A) pristine (B) etched, (C) PLL, (D) GO/PLL-H, and (E) GO/PLL-LbL FO membranes.

resulting breakage of surface covalent and hydrogen bonds leads to a looser ridge-valley structure than the pristine one (compare Figures 8A and 8B), confirming the surface roughness results detected by AFM. Only a slight change of the ridge-valley structure occurs after grafting with PLL (Figure 8C), and both membrane have skin layers from 100 to 200 nm. In contrast, the surface morphology of GO-PLL-H grafted membrane became highly compact with a skin layer thickness of 50−100 nm, resulting from better interface compatibility between the GO nanosheets/PLL and the PA skin layer as shown in Figure 8D. Although the GO nanosheets are visible, laying on the surface of GO-PLL-LbL grafted PA membrane, the surface morphology did not appear to be enhanced in the same way as for GO-PLL-H (Figure 8E), and the skin layer thickness is comparable to the pristine and etched membranes.

3.6. Contact Angle Analysis. It is well-known that the hydrophilic membrane surfaces have increased biofouling resistance properties.[12,32,43] As such, the captive bubble method was used to measure the surface hydrophilicity of pristine and grafted FO membranes. The etched membrane surface displayed a high hydrophobic nature of (73°), compared to the pristine (50°) case. This can be understood in light of the apparent roughness of the etched membrane. The surface hydrophilicity of the grafted PLL, GO/PLL-LbL, and GO/PLL-H membranes was improved by the modification to 42, 38, and 30°, respectively (Figure 9). The contact angle decrease with the incorporation of PLL and GO nanosheets is expected, as these are hydrophilic materials containing abundant amino, hydroxyl, and carboxylic acid functional groups

3.7. Performance Patterns of Tested Membranes. A flux decline resulted from the surface modification with PLL due to the additional mass deposited onto the active layer. In contrast, with GO/PLL surface modification the hydrophilic nature of GO nanosheets played an important role in maintaining the same J_w rate as the pristine sample (Figure 10), which is in agreement with contact angle results.

A second important flux parameter for FO membranes is the J_s. Economically speaking, the loss of draw solution is an

DOI: 10.1021/acsami.5b04818
ACS Appl. Mater. Interfaces 2015, 7, 18004−18016

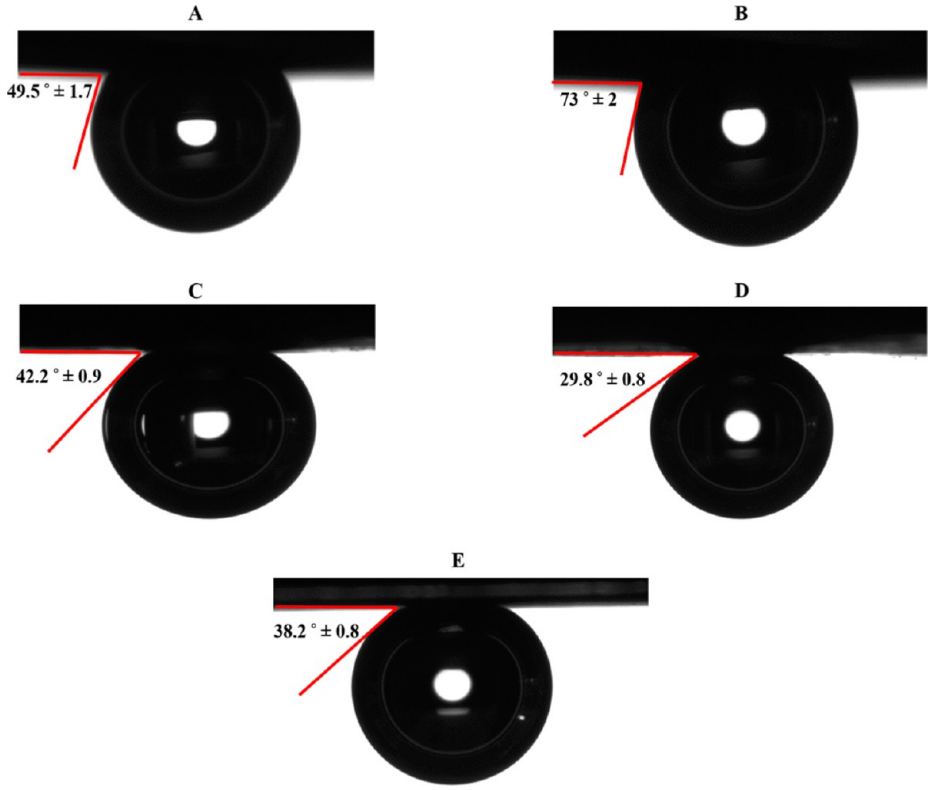

Figure 9. Contact angle measurements of (A) pristine, (B) etched, (C) PLL, (D) GO/PLL-H, and (E) GO/PLL-LbL FO membranes.

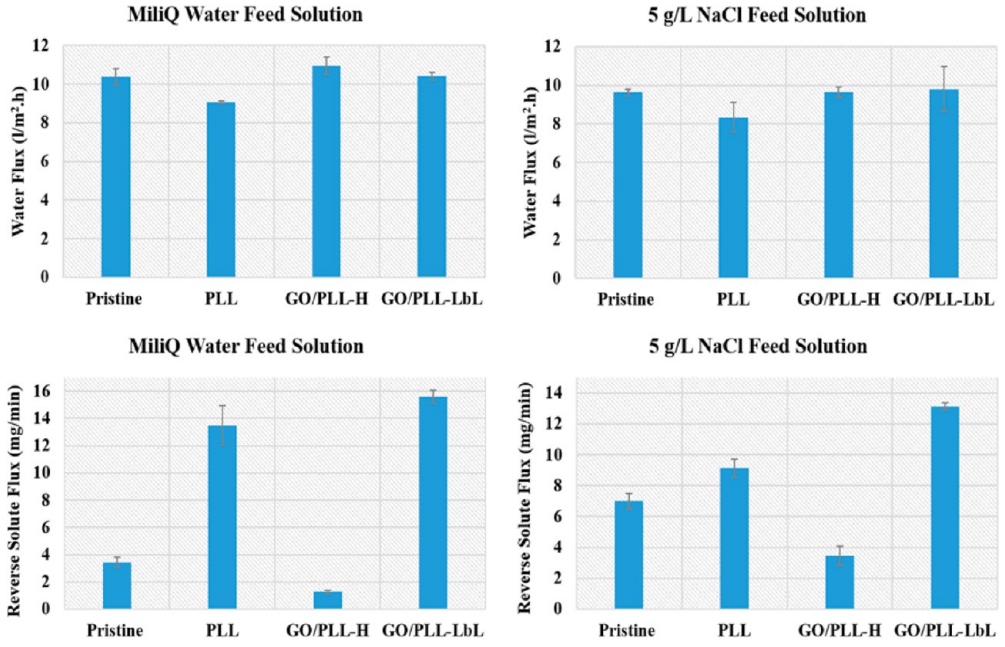

Figure 10. Water flux and reverse solute flux performance profile of the pristine and grafted membranes.

undesirable phenomenon that accelerates the onset of fouling and scaling on the active membrane layer. As shown in Figure 10, when Milli-Q water feed solution and 2 M NaCl draw solution was utilized, the J_s of the pristine membrane was 3.5 mg/min. The J_s of the grafted PLL and GO/PLL-LbL membranes increased by 74 and 78%, respectively, due to the significant swelling when in contact with high salt concentration (draw solution), leading to the formation of loose structures that accommodate salt ion diffusion[25,46] along with an increase in ICP. In contrast, the salt rejection performance of the GO/PLL-H was enhanced, and hence, the J_s of the GO/PLL-H declined by 63% compared to the pristine sample. Similar, though less extreme, reverse solute flux behavior was also observed when NaCl (5000 ppm) was used as a feed solution with both PLL and GO/PLL-LbL membranes having increased reverse solute flux compared to the pristine membrane, while the GO/PLL-H membrane was 50% reduced. This is as a result of tight active layer formation with the hybrid type modification

DOI: 10.1021/acsami.5b04818
ACS Appl. Mater. Interfaces 2015, 7, 18004−18016

and indicates that GO/PLL-H membrane modification provides superior salt rejection ability.

3.8. Evaluation of the Membranes Antibacterial Activity. *3.8.1. ATP Test.* The level of bacterial colonisation on fouled membranes was determined by the ATP bioluminescence assay test. The ATP concentration of the pristine, PLL, GO/PLL-LbL, and GO/PLL-H membranes were 28, 14.5, 14, and 0.1 μg/L, respectively (Figure 11). These results

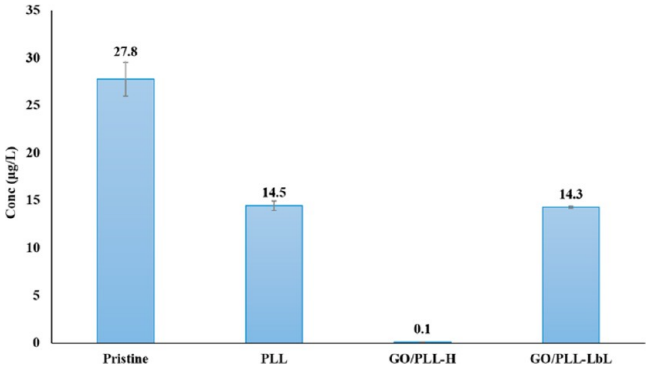

Figure 11. ATP concentrations of pristine and coated membranes.

confirm that PLL, GO/PLL-LbL, and GO/PLL-H modifications have a strong biocidal effect due to the antimicrobial effect of both PLL and GO nanosheets.[29,38,43,47,48] The significantly decreased bacterial survival on GO/PLL-H modified membranes compared to the pristine and other modifications is attributed to the synergism in the combination of a more compact, smoother and more hydrophilic surface holding a higher grafting density of GO nanosheets.

3.8.2. Biocidal Mechanism of GO/PLL. The superior biocidal and biofouling resistance properties of the GO/PLL-H-TFC membrane compared to that of the GO/PLL-LbL-TFC and PLL-TFC type could be attributed to the presence of both modifiers (PLL and GO) on the surface of hybrid modified membranes, which is not the case for the LbL and PLL modified types (Figure 12). In the hybrid membranes, both PLL and GO have a synergistic antibacterial mechanism. PLL is a cationic polypeptide which is considered as a superior model for bacterial cell toxicity[49−52] in which their positive amino groups cause electrostatic stacking at the negatively charged bacterial cell surface and result in the formation of huge aggregations.[53] This could lead in some cases to subsequent peptide translocation, membrane fusion, lipid phase transformation, and membrane lysis (Figure 12). Studies indicated that divalent cations and the Hep I and II phosphate groups in the bacterial lipopolysaccharide layer are critical cites for PLL binding efficiency.[54] Metabolomics analysis revealed that the PLL stress led to the inhibition of primary metabolic pathways through the suppression of the tricarboxylic acid cycle and glycolysis.[55]

Nevertheless, the amino groups binding mechanism alone may not be sufficient for the justification of the superior biocidal function of the GO/PLL-H-TFC membrane. Initially, the positive amino groups might be partially or entirely bound to the specific cellular acceptors, resulting in the expiration of the bacterial cells. Additionally, the GO sharp edges could simultaneously contribute to the biocidal effect, in which they destroy the cell membranes after partial penetration into the bacterial cells.[56] Once the GO and PLL bind and are inside the

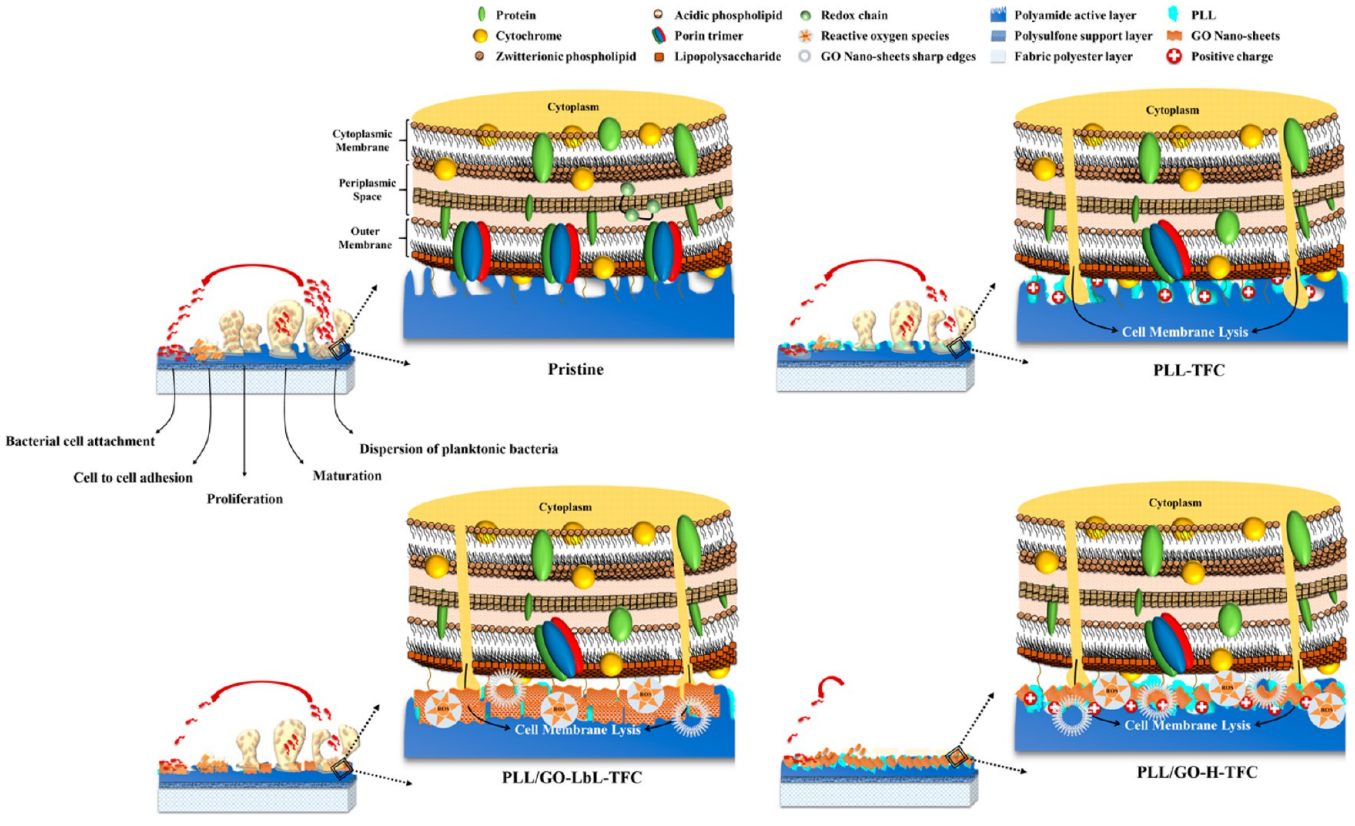

Figure 12. Schematic diagram illustrating the bacterial toxicity mechanism of pristine and grafted membranes.

DOI: 10.1021/acsami.5b04818
ACS Appl. Mater. Interfaces 2015, 7, 18004−18016

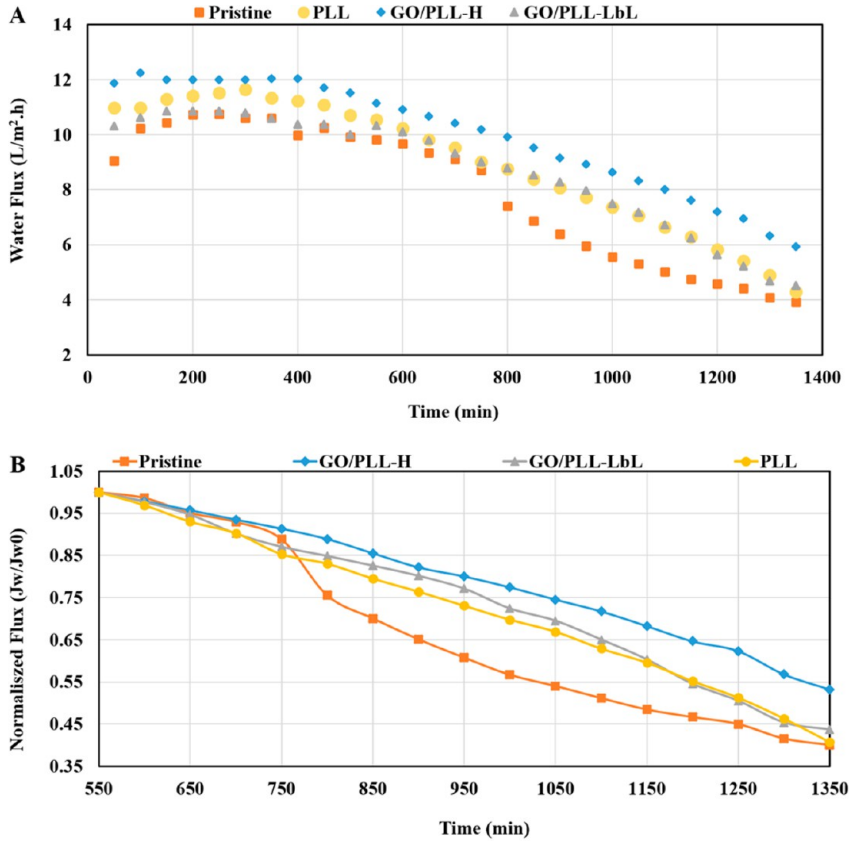

Figure 13. Results of accelerated biofouling experiment as a function of time in terms of (A) water flux and (B) normalized water flux of the pristine and coated membranes.

bacterial cell membrane, different cellular enzymatic systems could be inhibited or inactivated.

Moreover, the oxidative stress, which is a well-known antibacterial mechanism, normally caused by nanoparticles and particularly relevant for carbon-based nanomaterials,[57,58] is induced via the reactive oxygen species (ROS) generated by GO and contributes to their antibacterial activity.[59] Generally, oxidative stress induced by GO may be generated from several routes. In the first route, GO nanosheets directly produce ROS which mediate oxidative stress onto the bacterial cells.[60] The other route includes the indirect effect through the GO disturbance of a specific microbial process by interrupting or oxidizing an essential cellular structure or constituent in the absence of ROS generation. Accordingly, GO could also oxidize bacterial lipids, proteins, and DNA.[61]

3.8.3. Biofouling Propensity of Membranes. The water flux at a flow of 500 mL/min in the biofouling experiments for pristine, PLL, GO/PLL-H, and GO/PLL-LbL membranes is plotted in Figure 13A, experiments in which most of the decline in membrane water flux is attributed to the incremental growth of bacterial cells as a function of time. Under these conditions, each membrane roughly maintains flux for 400 min, after which flux steadily declines for modified membranes until the end of the experiment while the pristine membrane suffers a sudden flux drop at ~750 min. The normalized fluxes (J_w/J_{w0}) caused by biofouling of pristine and modified membranes were given in Figure 13B. The difference between pristine and modified membranes maximized at 950 min and at this time all grafted membranes showed significantly better biofouling resistance compared to the pristine; J_w/J_{w0} of pristine, PLL, GO/PLL-LbL, and GO/PLL-H membranes declined by 39, 27, 23, and 20%, respectively. At the end of the experiment, at 1350 min, the J_w/J_{w0} measurements of the pristine, PLL, and GO/PLL-LbL membranes had dropped by 60, 59, and 56%, respectively, illustrating that these two modified surfaces did not maintain notably improved biofouling resistance compared to the pristine sample over extended timeframes. In contrast, the GO/PLL-H membrane maintains relatively higher flux and only declined by 47% of its initial flux, demonstrating improved biofouling resistance performance. As such, these results are consistent with ATP analysis test, in which the GO/PLL-H membrane had the highest biocidal properties, leading to improved biofouling resistance, and reduced the interfacial adhesion between bacterial cells and membrane surface. Subsequent to the biofouling experiment, hydraulic cleaning using water at a flow rate of 1000 mL/min for 1 h allowed all membranes to recover their original water flux values.

4. CONCLUSION

We covalently attached GO nanosheets/PLL to the surface of FO membrane through hybrid or LbL approaches to form a stable modified surface of GO/PLL-H or GO/PLL-LbL membranes and tested their performance and biofouling resistance in FO mode. The grafting method used to incorporate GO nanosheets onto FO membrane surface played a significant role in its salt rejection behavior. Having GO nanosheets tightly bound to each other and to the membrane surface, as in the GO/PLL-H case, has improved the membrane surface morphology, smoothness, antibacterial properties, and hydrophilicity, resulting in the bifunctional benefit of both reduced loss of draw solution and increased biofouling

DOI: 10.1021/acsami.5b04818
ACS Appl. Mater. Interfaces 2015, 7, 18004−18016

resistance. Consequently, this easy and stable modification has the great potential to be applied in industrial applications of FO membrane filtration.

AUTHOR INFORMATION

Corresponding Author

*Tel: +61 8 8302 3517. Fax: +61 8 8302 5639. E-mail: milena.ginic-markovic@unisa.edu.au.

Notes

The authors declare no competing financial interest.

ACKNOWLEDGMENTS

The authors acknowledge the Australian government for the financial support of an IPRS scholarship at the University of South Australia.

REFERENCES

(1) Shaffer, D. L.; Werber, J. R.; Jaramillo, H.; Lin, S.; Elimelech, M. Forward Osmosis: Where Are We Now? *Desalination* **2015**, *356*, 271−284.

(2) Achilli, A.; Cath, T. Y.; Marchand, E. A.; Childress, A. E. The Forward Osmosis Membrane Bioreactor: A Low Fouling Alternative to MBR Processes. *Desalination* **2009**, *239*, 10−21.

(3) McGinnis, R. L.; Elimelech, M. Energy Requirements of Ammonia−carbon Dioxide Forward Osmosis Desalination. *Desalination* **2007**, *207*, 370−382.

(4) Mi, B.; Elimelech, M. Organic Fouling of Forward Osmosis Membranes: Fouling Reversibility and Cleaning without Chemical Reagents. *J. Membr. Sci.* **2010**, *348*, 337−345.

(5) ElMekawy, A.; Hegab, H. M.; Pant, D. The near-Future Integration of Microbial Desalination Cells with Reverse Osmosis Technology. *Energy Environ. Sci.* **2014**, *7*, 3921−3933.

(6) Otto, M. Staphylococcal Infections: Mechanisms of Biofilm Maturation and Detachment as Critical Determinants of Pathogenicity. *Annu. Rev. Med.* **2013**, *64*, 175−188.

(7) Worthley, C. H.; Constantopoulos, K. T.; Ginic-Markovic, M.; Pillar, R. J.; Matisons, J. G.; Clarke, S. Surface Modification of Commercial Cellulose Acetate Membranes Using Surface-Initiated Polymerization of 2-Hydroxyethyl Methacrylate to Improve Membrane Surface Biofouling Resistance. *J. Membr. Sci.* **2011**, *385−386*, 30−39.

(8) Chen, L.; Wen, Y. The Role of Bacterial Biofilm in Persistent Infections and Control Strategies. *Int. J. Oral Sci.* **2011**, *3*, 66−73.

(9) Pasmore, M.; Todd, P.; Smith, S.; Baker, D.; Silverstein, J.; Coons, D.; Bowman, C. N. Effects of Ultrafiltration Membrane Surface Properties on *Pseudomonas Aeruginosa* Biofilm Initiation for the Purpose of Reducing Biofouling. *J. Membr. Sci.* **2001**, *194*, 15−32.

(10) Habimana, O.; Semião, A. J. C.; Casey, E. The Role of Cell-Surface Interactions in Bacterial Initial Adhesion and Consequent Biofilm Formation on Nanofiltration/reverse Osmosis Membranes. *J. Membr. Sci.* **2014**, *454*, 82−96.

(11) Madaeni, S. S.; Ghaemi, N. Characterization of Self-Cleaning RO Membranes Coated with TiO_2 Particles under UV Irradiation. *J. Membr. Sci.* **2007**, *303*, 221−233.

(12) Hegab, H. M.; Wimalasiri, Y.; Ginic-Markovic, M.; Zou, L. Improving the Fouling Resistance of Brackish Water Membranes via Surface Modification with Graphene Oxide Functionalized Chitosan. *Desalination* **2015**, *365*, 99−107.

(13) Araújo, P. A.; Miller, D. J.; Correia, P. B.; van Loosdrecht, M. C. M.; Kruithof, J. C.; Freeman, B. D.; Paul, D. R.; Vrouwenvelder, J. S. Impact of Feed Spacer and Membrane Modification by Hydrophilic, Bactericidal and Biocidal Coating on Biofouling Control. *Desalination* **2012**, *295*, 1−10.

(14) Greenlee, L. F.; Lawler, D. F.; Freeman, B. D.; Marrot, B.; Moulin, P. Reverse Osmosis Desalination: Water Sources, Technology, and Today's Challenges. *Water Res.* **2009**, *43*, 2317−2348.

(15) Fritzmann, C.; Löwenberg, J.; Wintgens, T.; Melin, T. State-of-the-Art of Reverse Osmosis Desalination. *Desalination* **2007**, *216*, 1−76.

(16) Zou, S.; Gu, Y.; Xiao, D.; Tang, C. Y. The Role of Physical and Chemical Parameters on Forward Osmosis Membrane Fouling during Algae Separation. *J. Membr. Sci.* **2011**, *366*, 356−362.

(17) Tan, C. H.; Ng, H. Y. Revised External and Internal Concentration Polarization Models to Improve Flux Prediction in Forward Osmosis Process. *Desalination* **2013**, *309*, 125−140.

(18) Hancock, N. T.; Cath, T. Y. Solute Coupled Diffusion in Osmotically Driven Membrane Processes. *Environ. Sci. Technol.* **2009**, *43*, 6769−6775.

(19) Cornelissen, E.; Harmsen, D.; Dekorte, K.; Ruiken, C.; Qin, J.; Oo, H.; Wessels, L. Membrane Fouling and Process Performance of Forward Osmosis Membranes on Activated Sludge. *J. Membr. Sci.* **2008**, *319*, 158−168.

(20) Lee, S.; Boo, C.; Elimelech, M.; Hong, S. Comparison of Fouling Behavior in Forward Osmosis (FO) and Reverse Osmosis (RO). *J. Membr. Sci.* **2010**, *365*, 34−39.

(21) Nair, R. R.; Wu, H. A.; Jayaram, P. N.; Grigorieva, I. V.; Geim, A. K. Unimpeded Permeation of Water through Helium-Leak-Tight Graphene-Based Membranes. *Science (Washington, DC, U. S.)* **2012**, *335*, 442−444.

(22) Kannam, S. K.; Todd, B. D.; Hansen, J. S.; Daivis, P. J. Interfacial Slip Friction at a Fluid-Solid Cylindrical Boundary. *J. Chem. Phys.* **2012**, *136*, 244704.

(23) Han, Y.; Xu, Z.; Gao, C. Ultrathin Graphene Nanofiltration Membrane for Water Purification. *Adv. Funct. Mater.* **2013**, *23*, 3693−3700.

(24) Joshi, R. K.; Carbone, P.; Wang, F. C.; Kravets, V. G.; Su, Y.; Grigorieva, I. V.; Wu, H. A.; Geim, A. K.; Nair, R. R. Precise and Ultrafast Molecular Sieving through Graphene Oxide Membranes. *Science* **2014**, *343*, 752−754.

(25) Hu, M.; Mi, B. Layer-by-Layer Assembly of Graphene Oxide Membranes via Electrostatic Interaction. *J. Membr. Sci.* **2014**, *469*, 80−87.

(26) Szabó, T.; Berkesi, O.; Forgó, P.; Josepovits, K.; Sanakis, Y.; Petridis, D.; Dékány, I. Evolution of Surface Functional Groups in a Series of Progressively Oxidized Graphite Oxides. *Chem. Mater.* **2006**, *18*, 2740−2749.

(27) Li, D.; Müller, M. B.; Gilje, S.; Kaner, R. B.; Wallace, G. G. Processable Aqueous Dispersions of Graphene Nanosheets. *Nat. Nanotechnol.* **2008**, *3*, 101−105.

(28) Hu, M.; Mi, B. Enabling Graphene Oxide Nanosheets as Water Separation Membranes. *Environ. Sci. Technol.* **2013**, *47*, 3715−3723.

(29) Hu, W.; Peng, C.; Luo, W.; Lv, M.; Li, X.; Li, D.; Huang, Q.; Fan, C. Graphene-Based Antibacterial Paper. *ACS Nano* **2010**, *4*, 4317−4323.

(30) Santos, C. M.; Mangadlao, J.; Ahmed, F.; Leon, A.; Advincula, R. C.; Rodrigues, D. F. Graphene Nanocomposite for Biomedical Applications: Fabrication, Antimicrobial and Cytotoxic Investigations. *Nanotechnology* **2012**, *23*, 395101.

(31) Mi, B.; Elimelech, M. Chemical and Physical Aspects of Organic Fouling of Forward Osmosis Membranes. *J. Membr. Sci.* **2008**, *320*, 292−302.

(32) Boo, C.; Elimelech, M.; Hong, S. Fouling Control in a Forward Osmosis Process Integrating Seawater Desalination and Wastewater Reclamation. *J. Membr. Sci.* **2013**, *444*, 148−156.

(33) Nguyen, A.; Zou, L.; Priest, C. Evaluating the Antifouling Effects of Silver Nanoparticles Regenerated by TiO_2 on Forward Osmosis Membrane. *J. Membr. Sci.* **2014**, *454*, 264−271.

(34) Pacheco, F. A.; Pinnau, I.; Reinhard, M.; Leckie, J. O. Characterization of Isolated Polyamide Thin Films of RO and NF Membranes Using Novel TEM Techniques. *J. Membr. Sci.* **2010**, *358*, 51−59.

(35) Hijnen, W. A. M.; Biraud, D.; Cornelissen, E. R.; van der Kooij, D. Threshold Concentration of Easily Assimilable Organic Carbon in Feedwater for Biofouling of Spiral-Wound Membranes. *Environ. Sci. Technol.* **2009**, *43*, 4890−4895.

DOI: 10.1021/acsami.5b04818
ACS Appl. Mater. Interfaces 2015, 7, 18004−18016

(36) Hijnen, W. A. M.; Cornelissen, E. R.; van der Kooij, D. Threshold Concentrations of Biomass and Iron for Pressure Drop Increase in Spiral-Wound Membrane Elements. *Water Res.* **2011**, *45*, 1607−1616.
(37) Tiraferri, A.; Kang, Y.; Giannelis, E. P.; Elimelech, M. Highly Hydrophilic Thin-Film Composite Forward Osmosis Membranes Functionalized with Surface-Tailored Nanoparticles. *ACS Appl. Mater. Interfaces* **2012**, *4*, 5044−5053.
(38) Reuter, M.; Schwieger, C.; Meister, A.; Karlsson, G.; Blume, A. Poly-L-Lysines and Poly-L-Arginines Induce Leakage of Negatively Charged Phospholipid Vesicles and Translocate through the Lipid Bilayer upon Electrostatic Binding to the Membrane. *Biophys. Chem.* **2009**, *144*, 27−37.
(39) Ettori, A.; Gaudichet-Maurin, E.; Schrotter, J.-C.; Aimar, P.; Causserand, C. Permeability and Chemical Analysis of Aromatic Polyamide Based Membranes Exposed to Sodium Hypochlorite. *J. Membr. Sci.* **2011**, *375*, 220−230.
(40) KWON, Y.; LECKIE, J. Hypochlorite Degradation of Crosslinked Polyamide membranesII. Changes in Hydrogen Bonding Behavior and Performance. *J. Membr. Sci.* **2006**, *282*, 456−464.
(41) Chen, C.; Li, J.; Li, R.; Xiao, G.; Yan, D. Synthesis of Superior Dispersions of Reduced Graphene Oxide. *New J. Chem.* **2013**, *37*, 2778−2783.
(42) Ginic-Markovic, M.; Barclay, T. G.; Constantopoulos, K. T.; Markovic, E.; Clarke, S. R.; Matisons, J. G. Biofouling Resistance of Polysulfobetaine Coated Reverse Osmosis Membranes. *Desalination* **2015**, *369*, 37−45.
(43) Hegab, H. M.; Zou, L. Graphene Oxide-Assisted Membranes: Fabrication and Potential Applications in Desalination and Water Purification. *J. Membr. Sci.* **2015**, *484*, 95−106.
(44) Kochkodan, V. M.; Hilal, N.; Goncharuk, V. V.; Al-Khatib, L.; Levadna, T. I. Effect of the Surface Modification of Polymer Membranes on Their Microbiological Fouling. *Colloid J.* **2006**, *68*, 267−273.
(45) Do, V. T.; Tang, C. Y.; Reinhard, M.; Leckie, J. O. Degradation of Polyamide Nanofiltration and Reverse Osmosis Membranes by Hypochlorite. *Environ. Sci. Technol.* **2012**, *46*, 852−859.
(46) Dubas, S. T.; Schlenoff, J. B. Polyelectrolyte Multilayers Containing a Weak Polyacid: Construction and Deconstruction. *Macromolecules* **2001**, *34*, 3736−3740.
(47) Sreeprasad, T. S.; Maliyekkal, M. S.; Deepti, K.; Chaudhari, K.; Xavier, P. L.; Pradeep, T. Transparent, Luminescent, Antibacterial and Patternable Film Forming Composites of Graphene Oxide/reduced Graphene Oxide. *ACS Appl. Mater. Interfaces* **2011**, *3*, 2643−2654.
(48) Mejías Carpio, I. E.; Santos, C. M.; Wei, X.; Rodrigues, D. F. Toxicity of a Polymer-Graphene Oxide Composite against Bacterial Planktonic Cells, Biofilms, and Mammalian Cells. *Nanoscale* **2012**, *4*, 4746−4756.
(49) Matsuzaki, K.; Murase, O.; Miyajima, K. Kinetics of Pore Formation by an Antimicrobial Peptide, Magainin 2, in Phospholipid Bilayers. *Biochemistry* **1995**, *34*, 12553−12559.
(50) Pokorny, A.; Birkbeck, T. H.; Almeida, P. F. F. Mechanism and Kinetics of Delta-Lysin Interaction with Phospholipid Vesicles. *Biochemistry* **2002**, *41*, 11044−11056.
(51) Liu, H.; Pei, H.; Han, Z.; Feng, G.; Li, D. The Antimicrobial Effects and Synergistic Antibacterial Mechanism of the Combination of E-Polylysine and Nisin against *Bacillus subtilis*. *Food Control* **2015**, *47*, 444−450.
(52) Ye, R.; Xu, H.; Wan, C.; Peng, S.; Wang, L.; Xu, H.; Aguilar, Z. P.; Xiong, Y.; Zeng, Z.; Wei, H. Antibacterial Activity and Mechanism of Action of E-Poly-L-Lysine. *Biochem. Biophys. Res. Commun.* **2013**, *439*, 148−153.
(53) Volodkin, D.; Ball, V.; Schaaf, P.; Voegel, J.-C.; Mohwald, H. Complexation of Phosphocholine Liposomes with Polylysine. Stabilization by Surface Coverage versus Aggregation. *Biochim. Biophys. Acta, Biomembr.* **2007**, *1768*, 280−290.
(54) Hyldgaard, M.; Mygind, T.; Vad, B. S.; Stenvang, M.; Otzen, D. E.; Meyer, R. L. The Antimicrobial Mechanism of Action of Epsilon-Poly-L-Lysine. *Appl. Environ. Microbiol.* **2014**, *80*, 7758−7770.
(55) Bo, T.; Liu, M.; Zhong, C.; Zhang, Q.; Su, Q.-Z.; Tan, Z.-L.; Han, P.-P.; Jia, S.-R. Metabolomic Analysis of Antimicrobial Mechanisms of ε-Poly-L-Lysine on *Saccharomyces cerevisiae*. *J. Agric. Food Chem.* **2014**, *62*, 4454−4465.
(56) Akhavan, O.; Ghaderi, E. Toxicity of Graphene and Graphene Oxide Nanowalls against Bacteria. *ACS Nano* **2010**, *4*, 5731−5736.
(57) Wang, G.; Yang, J.; Park, J.; Gou, X.; Wang, B.; Liu, H.; Yao, J. Facile Synthesis and Characterization of Graphene Nanosheets. *J. Phys. Chem. C* **2008**, *112*, 8192−8195.
(58) Kang, S.; Pinault, M.; Pfefferle, L. D.; Elimelech, M. Single-Walled Carbon Nanotubes Exhibit Strong Antimicrobial Activity. *Langmuir* **2007**, *23*, 8670−8673.
(59) Sanchez, V. C.; Jachak, A.; Hurt, R. H.; Kane, A. B. Biological Interactions of Graphene-Family Nanomaterials: An Interdisciplinary Review. *Chem. Res. Toxicol.* **2012**, *25*, 15−34.
(60) Zhang, Y.; Ali, S. F.; Dervishi, E.; Xu, Y.; Li, Z.; Casciano, D.; Biris, A. S. Cytotoxicity Effects of Graphene and Single-Wall Carbon Nanotubes in Neural Phaeochromocytoma-Derived PC12 Cells. *ACS Nano* **2010**, *4*, 3181−3186.
(61) Liu, S.; Zeng, T. H.; Hofmann, M.; Burcombe, E.; Wei, J.; Jiang, R.; Kong, J.; Chen, Y. Antibacterial Activity of Graphite, Graphite Oxide, Graphene Oxide, and Reduced Graphene Oxide: Membrane and Oxidative Stress. *ACS Nano* **2011**, *5*, 6971−6980.

DOI: 10.1021/acsami.5b04818
ACS Appl. Mater. Interfaces 2015, 7, 18004−18016